Materials for life sciences

Alendronate-loaded gelatin microparticles as templating agents for macroporous magnesium phosphate-based bone cements

Rita Gelli[1], Lucrezia Sforzi[1], Francesco Montanari[1], Francesca Ridi[1,*] (iD), and Piero Baglioni[1]

[1] *Department of Chemistry "Ugo Schiff" and CSGI, University of Florence, Via della Lastruccia 3, Sesto Fiorentino, 50019 Florence, Italy*

ABSTRACT

Magnesium phosphate-based cements (MPCs) have recently attracted great attention as materials for bone repair. However, the lack of macroporosity, fundamental for cells permeation and bone ingrowth, is one of the main limitations hampering MPCs full exploitation. In this work gelatin microparticles are exploited as templating agents for the creation of macroporosities in MPCs. In addition, gelatin particles were loaded with a well-recognized drug for the treatment of osteoporosis, alendronate, to locally release the therapeutic agent. Gelatin microparticles of different size were prepared with a simple water-in-oil emulsion method and included in MPCs at various concentrations. The properties of both the MPCs and the final material were characterized by assessing the composite in terms of injectability, setting time, infrared spectroscopy, scanning electron microscopy and confocal Raman microscopy. The MPC-gelatin composites were then incubated in water at physiological temperature, to promote the dissolution of the gelatin, obtain a macroporous cement, and release gelatin and alendronate. The obtained results show that gelatin microparticles have a twofold action as they allow for the formation of MPC with an interconnected and hundreds of μm-sized porosity and the local release of alendronate, resulting in a material with ideal features for bone repair.

GRAPHICAL ABSTRACT
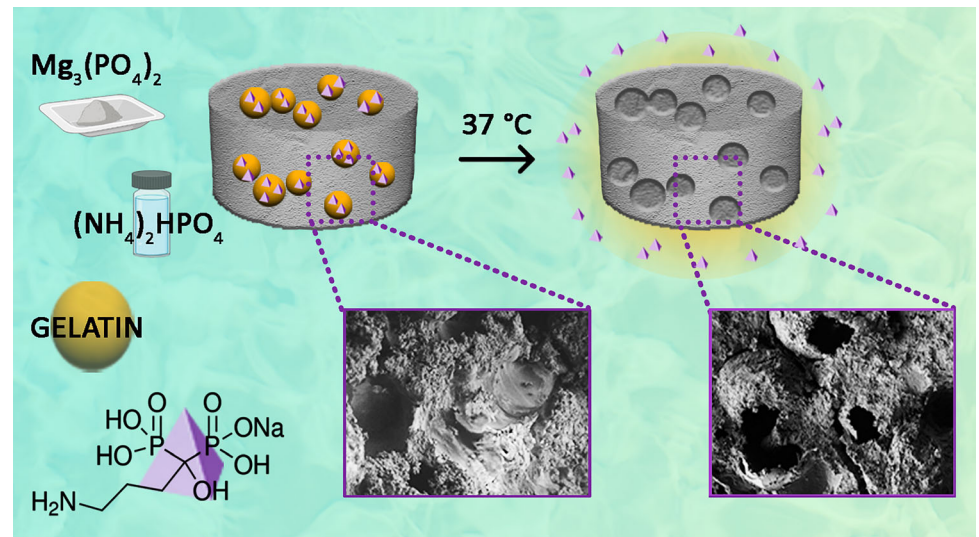
Introduction

Bone defects and diseases are among the major medical concerns due to the increase of the average age of the population in developed countries [1]. The design of innovative bone repair solutions is an open challenge [2, 3] and, among the different synthetic materials to face this issue, bone cements hold an important position [4, 5], particularly when minimally invasive treatments are sought (i.e., bone augmentation and reconstruction procedures, such as maxillofacial procedures or vertebroplasty [6]). According to IUPAC, bone cements are defined as synthetic, self-curing organic or inorganic materials used to fill up a cavity or to create a mechanical fixation [7]. Among the inorganic ones, the most important are based on phosphates, namely Calcium Phosphate Cements (CPCs) [8] and Magnesium Phosphate Cements (MPCs) [9]. The use of CPCs in the biomedical field is widespread due to their chemical similarity with bone inorganic matrix, which confers them excellent biocompatibility. Other advantages include the handling properties and the ability to set in physiological conditions, whereas phase separation during injection, poor in vivo resorption rate and scarce mechanical properties are

regarded as the main drawbacks of these materials [5, 9]. MPCs, which have a long history as construction materials in civil engineering [10], could represent a valuable alternative to CPCs, as they display faster setting, higher early strength and superior degradation behavior while maintaining a good biocompatibility [9, 11]. In addition, in vitro studies suggest that Mg^{2+} ions stimulate osteoblast differentiation and inhibit osteoclast formation [12] and preliminary in vivo applications of MPCs are promising [11, 13].

Despite the great number of appealing features of phosphate-based cements for biomedical applications, one of the major limitations of both CPCs and MPCs is their lack of macroporosity [6, 14–16]. While such cements display intrinsic microporosities, which allow for protein adsorption, cell attachment and permeability of the material to body fluids, they typically lack of interconnected macropores over 100 μm which would allow for angiogenesis and bone ingrowth, promoting the fast resorption of the cement [17]. Several approaches have been described in the literature to obtain macroporosities in phosphate-based cements. For CPCs, macropores were obtained by foaming [18–20], using porogens such as mannitol [21, 22], frozen sodium phosphate solutions [23], tri-calcium phosphate granules [24] and sucrose

fatty acid esters [14]. Despite these efforts, none of the commercially available CPCs offers the possibility of macropore formation [17], suggesting the need to develop more effective strategies to prepare these systems in a more feasible way.

Macroporous MPCs have been investigated to a lesser extent: the first reports include foaming with zinc powder [25], also combined with a chemical foaming agent [26], sodium bicarbonate [27] or protein-based foaming agents [28], even if none of these materials was designed for biomedical applications. In the orthopedic field, macroporous MPCs were obtained using biodegradable Mg particles as porogens during cement setting [29] or polyurethane foams [30].

Among the possible methods to create macroporosities in MPCs, the inclusion of sacrificial polymeric microspheres is an underexplored yet promising strategy. The idea behind this approach is the use of polymeric microspheres able to degrade or dissolve in physiological conditions, to be mixed with the cement paste: when the composite is applied in vivo, the dissolution of the microspheres should lead to a macroporous cement in which bone cells could easily penetrate and grow, forming new bone tissue. Among the polymers which can be used to this purpose, gelatin is one of the most suitable as it derives from the hydrolysis of collagen, which is the main component of bone organic matrix. Gelatin is biocompatible and widely used in a variety of fields including the production of scaffolds and hydrogels for tissue engineering, in pharmaceutics, cosmetics and food industry [31]. Moreover, gelatin can easily be shaped in nano [32] and microparticles [33], and hydrogels undergo a *gel–sol* transition at about 37 °C, making them ideal candidates to prepare templating particles for macroporous cements. Gelatin microparticles were already included in CPCs [34–41], but only a very recent work reports their use in MPCs [42]. In addition to the creation of macroporosities, an advantage of including gelatin microspheres in bone cements is the possibility to load them with drugs that, upon dissolution of the gelatin component, can be released in the surroundings of the site of application of the cement, providing an in situ therapeutic action. For the treatment of bone disorders and osteoporosis, bisphosphonates and in particular alendronate (ALN) represent the standard therapy, inhibiting bone loss by reducing osteoclasts activity [1]. Since the systemic administration of ALN is known to display several undesirable side effects (gastrointestinal diseases, fever, articular pain), the development of strategies to locally administrate such drug is an urgent need [43]. In this scenario, ALN in gelatin microspheres could be an innovative way to deliver the drug directly in the site of action: the inclusion in the microspheres rather than the direct mixing with the cement powder should be preferred as, in principle, it should avoid the burst release [42]; in addition, for CPCs it is reported that ALN interaction with the cement powder affects the setting time of the paste and worsens the final mechanical properties [1]. The inclusion of ALN in CPCs is well described in the literature [44–48] while, to the best of our knowledge, no investigations of ALN in MPCs are reported.

This work describes the design of a MPC in which gelatin microparticles act both as porogens and as agents for the loading and release of ALN. Gelatin microparticles of different size were prepared through a simple emulsion procedure by varying the stirring speed. MPCs were synthesized upon reaction of TMP (tri-magnesium phosphate) and aqueous solutions of DAHP (Di-Ammonium Hydrogen Phosphate), including differently sized gelatin microparticles, and the properties of the hybrid inorganic–organic composite were analyzed. Cements were then incubated in physiological conditions, and the resulting macroporosity was assessed, together with the release profile of gelatin and ALN. To the best of our knowledge, this is the first study in which gelatin microparticles of different sizes and loaded with an anti-osteoporotic drug are included in TMP-based MPCs, representing an advancement in the field of functional biomaterials for orthopedic applications.

Materials and methods

Materials

Gelatin from porcine skin, type A, and $Mg(OH)_2$ (purity $\geq$ 95%) were obtained from Fluka, while $MgHPO_4 \cdot 3H_2O$ (Newberyite, purity $\geq$ 97%) was purchased from Aldrich. $(NH_4)_2HPO_4$, (DAHP, Di-Ammonium Hydrogen Phosphate, purity $\geq$ 99%) was obtained from Riedel de Haën. A commercial extra virgin olive oil was used to prepare gelatin microparticles, whereas acetone (purity $\geq$ 99.8%) and

isopropyl alcohol (purity ≥ 99.8%) were purchased from Carlo Erba. Alendronate sodium trihydrate (purity 97%) was obtained from Alfa Aesar. For the preparation of the Biuret reagent, $CuSO_4$ (purity > 98%) was obtained from Carlo Erba, $KNaC_4H_4O_6 \cdot 4H_2O$ (purity > 99%) and NaOH (purity > 99%) were purchased from Sigma-Aldrich, while KI (purity > 99%) from Fluka. For alendronate quantification, $FeCl_3 \cdot 6H_2O$ (purity 97%) was obtained from Sigma-Aldrich, and $HClO_4$ 70% from Merck. De-ionized water was used during all the experiments. All reagents were used without further purification.

Preparation of gelatin microparticles and loading with alendronate

Gelatin microspheres were prepared by re-adapting a protocol from the literature [49]. 1 g of gelatin was dissolved in 9 mL of water under stirring at 50 °C, while 40 mL of olive oil were separately heated at the same temperature in a beaker. Gelatin solution was dropwise added to the olive oil, and a water-in-oil (W/O) emulsion was obtained. The procedure was repeated four times using different stirring speeds (200, 500, 800 and 1100 rpm), which correspond to samples labeled as G200, G500, G800 and G1100, respectively. After about 5 min from the gelatin addition, the W/O emulsion was cooled down to ~ 10 °C, while maintaining the selected stirring speed. The resulting gelatin microspheres were then collected by means of a vacuum filtration and a Büchner funnel using Whatman filter paper (grade 50) and thoroughly washed with acetone. The obtained microparticles were dried overnight at room temperature, and then were sieved using a 1 mm mesh-sized sieve, to remove large aggregates.

The loading procedure of ALN was carried out only with G500 and G800 samples, which were selected to prepare cements based on the experimental results (see "Characterization of gelatin microparticles" section). 100 mg of gelatin microparticles were dispersed in 10 mL of an aqueous solution 10 mg/mL of ALN. The dispersion was kept under moderate stirring at 15 °C for 2 h. The microparticles were separated by means of vacuum filtration with a Büchner funnel using Whatman filter paper and dried overnight at room temperature. The dried microparticles were gently grinded with mortar and

pestle to crumble large aggregates, finally obtaining samples G500_ALN and G800_ALN.

Preparation of MPCs-gelatin

MPCs were prepared upon reaction of TMP ($Mg_3(PO_4)_2$, Tri-Magnesium Phosphate) and aqueous solutions of DAHP (($NH_4)_2HPO_4$, Di-Ammonium Hydrogen Phosphate) [50]. TMP was prepared by means of a calcination reaction between $MgHPO_4 \cdot 3H_2O$ and $Mg(OH)_2$, in molar ratio 2:1 [51]. 52.3 g of $MgHPO_4 \cdot 3H_2O$ were carefully mixed with 8.75 g of $Mg(OH)_2$ and transferred in ceramic crucibles. The powder was heated in a muffle furnace (Nabertherm LT 5/13/B410) at 1000 °C for 5 h. After quenching at room temperature, the calcined product was crushed with mortar and pestle and sieved using a 150 μm sieve. The procedure is schematized in Fig. S1A.

Cements were prepared by mixing 0.3 g of the powder component (i.e., TMP and gelatin microspheres, G500 or G800) with 0.2 mL of an aqueous solution of DAHP, at powder to liquid (P/L) ratio of 1.5 and by keeping constant the ratio of TMP grams/mmoles DAHP = 0.43. For this reason, the concentration of DAHP solution was adjusted according to the amount of TMP used in the formulation (see Table 1). TMP and DAHP react while forming struvite ($MgNH_4PO_4 \cdot 6H_2O$) as the main binding phase [51].

Two sets of cements were prepared: i. "G" series, in which dried gelatin microspheres were carefully mixed with TMP powder before the addition of DAHP solution and ii. "GS" series, in which gelatin microspheres were swelled in DAHP solution (same amounts than "G" series, see Table 1) for 10 min and then mixed with TMP (see Figs. S1B and S1C). In all cases, the resulting pastes were mixed for about 30 s and placed in plastic molds of 9 mm diameter. The cements were allowed to set at 37 °C and relative humidity > 96% for at least 7 days before characterization.

The same procedure was followed to prepare MPCs with ALN-loaded microparticles, using G500_ALN and G800_ALN instead of G500 and G800. For the release experiments (see "Quantification of gelatin" section), a reference specimen where ALN was mixed as a powder with TMP before DAHP addition was prepared (G0_ALN). For this sample, 0.3 g of TMP were mixed with 23 mg ALN before the addition of 200 μL DAHP 3.5 M. The

Table 1 Composition of samples under investigation in this study

Sample	TMP (g)	Gelatin microspheres (g)	% Gelatin/powders*	DAHP (M)†
G0	0.3	–	0	3.5
G500_5%	0.285	0.015	5	3.33
G500_15%	0.255	0.045	15	2.98
G500_25%	0.225	0.075	25	2.63
G800_5%	0.285	0.015	5	3.33
G800_15%	0.255	0.045	15	2.98
G800_25%	0.225	0.075	25	2.63

*Powders refer to the sum of TMP and gelatin microspheres

†The concentration of DAHP solution is chosen to keep constant in all samples the amount of TMP with respect to DAHP (grams TMP/mmoles DAHP = 0.43)

amount of ALN was chosen to match that in cements prepared with ALN-loaded microparticles.

Characterization techniques

Field emission-scanning electron microscopy (FE-SEM)

The morphology of the samples was examined by means of Field Emission-Scanning Electron Microscopy (FE-SEM). Dried gelatin microparticles or cross sections of the cements were fixed on aluminum stubs by means of conductive tape. The measurements were taken with a Zeiss ΣIGMA FE-SEM (Carl Zeiss Microscopy GmbH), with an accelerating voltage of 2.0 kV, a sample-detector distance ∼ 4 mm and using the secondary electrons detector. The size distribution curves of different samples were obtained by measuring the diameter of about 200 particles *per* sample using the software ImageJ.

Laser granulometry

The size distribution of dried gelatin microparticles was analyzed by means of laser granulometry, using a Mastersizer 3000 (Malvern) with a Hydro SM dispersion unit. Isopropyl alcohol (refractive index at 20 °C: 1.375) was used as dispersant, while the optical properties of gelatin were: density 1.27 g/mL, absorption coefficient 0.01, refractive index 1.52. Measurements were conducted using a stirring speed of 1800 rpm, and for each sample 20 runs of 5 s each (and 5 s of delay) were averaged. Before adding the sample, the background (isopropyl alcohol) was measured for 15 s, then gelatin microparticles were added until an obscuration of ∼ 4% was attained. The results are expressed as D_{10}, D_{50} and D_{90} (average ± standard deviation of 20 measurements).

Thermogravimetry (TGA)

Thermal analysis was carried out using a Simultaneous Thermogravimetry/Differential Scanning Calorimetry (TGA/DSC) SDT Q600 from TA Instruments. Samples were placed in alumina pans and measured in N_2 atmosphere (flow rate 100 mL/min) from room temperature to 1000 °C, with a ramp of 10 °C/min.

Setting time

The initial and final setting times of the pastes were obtained using a Gillmore apparatus (Matest), following the ASTM standard C-266. MPCs-gelatin cements were prepared according to Table 1 and immediately placed in plastic molds; the setting occurred at $T = 37$ °C and relative humidity > 96% and, every minute, samples were removed from the incubation chamber and tested with the Gillmore apparatus. The cement is considered to have reached its initial or final setting time when its surface, respectively, bears the initial or final Gillmore needle without appreciable indentation (initial needle ϕ = 2.12 mm, weight 113 g and final needle ϕ = 1.06 mm, weight 453.6 g).

Attenuated total reflection-fourier transform infrared spectroscopy (ATR-FTIR)

ATR-FTIR spectra of the cements were acquired by means of a Nexus Thermo-Nicolet 870 FT-IR spectrophotometer equipped with a MCT detector and a Golden Gate. The spectra were collected in the 4000–650 cm^{-1} range, with 128 scans and resolution 2 cm^{-1}.

Confocal Raman microscopy

Confocal Raman microscopy was carried out using a Renishaw InVia^{TM} Qontor confocal microRaman system. Maps were collected using a 20X objective and a laser operating at 785 nm with a power of 10% of its maximum, which is 100 mW. For each sample, a montage of 3 × 3 images was used to image an area of 180 × 100 μm. Each spectrum was acquired for 1 s and 5 accumulations in LiveTrack^{TM} mode, in order to keep the focus of samples' surface and follow its roughness. Spectra were processed with the Renishaw software WiRE, corrected for cosmic rays, baseline and noise, and then used to obtain maps based on the signal-to-baseline intensity from 910 to 970 cm^{-1} for struvite, 970–1050 cm^{-1} for TMP and 1350–1500 cm^{-1} for gelatin.

X-ray micro-computed tomography (micro-CT)

X-ray microtomography was performed with a SKYSCAN 1172 high-resolution XμCT scanner (Bruker) on samples G0 and G800_25%_ALN after the dissolution experiment (see "Dissolution experiments" section). Experiments were performed using an X-ray source at 100 kV and 100 μA. For G0, the sample-source distance was 83.54 mm (pixel size: 8.94 μm) while for G800_25% the sample-source distance was 72.29 mm (pixel size: 7.73 μm). Reconstruction, 3D visualization and analysis of the micro-CT images were performed using, respectively, the software NRecon, CTvox and CTAn (Skyscan, Bruker).

Dissolution experiments

MPC-gelatin samples, prepared as described in "Preparation of MPCs-gelatin" section using microspheres loaded with ALN, were incubated in water (20 mL) at 37 °C for 12 days to determine the extent of their dissolution. Samples were visually inspected daily and, at the end of the experiment, they were dried in oven at 37 °C for 1 week. The weight of the dried samples (w_f, final weight) was compared to the weight before incubation (w_i, initial weight) and the weight loss was expressed as (Eq. 1):

$$\text{Weight loss \%} = \frac{(w_i - w_f)}{w_i} \times 100 \qquad (1)$$

Dried MPCs were also imaged by means of FE-SEM and selected specimens also by means of X-ray microtomography. The amount of gelatin and ALN present in the incubation medium at the end of the experiment were analyzed spectrophotometrically with the methods described in "Quantification of gelatin" and "Quantification of ALN" section, respectively.

Quantification of gelatin

Gelatin concentration in water was determined spectrophotometrically with the Biuret method [52]. The Biuret reagent was prepared by dissolving 0.048 g of $CuSO_4$ and 0.3 g of $KNaC_4H_4O_6 \cdot 4H_2O$ in 15 mL of NaOH 10% w/v and adding water up to the final volume of 50 mL. 0.05 g of KI were finally added to prevent copper reduction. Gelatin standards in water in the range 0–10 mg/mL were prepared by means of serial dilutions, and the assay was carried out by reacting 0.4 mL of standard/sample with 2 mL of Biuret reagent. After 30 min, spectra were collected with a UV–Vis spectrophotometer Cary3500 (Agilent) between 400 and 800 nm, integration time 0.02 s, bandwidth 2 nm, using as a reference a sample composed of 0.4 mL water + 2 mL Biuret reagent. The absorbance at 540 nm was used to determine the calibration curve, which is shown in Fig. S2A.

Quantification of ALN

ALN concentration in water was analyzed by using the formation of a Fe(III)-ALN complex that absorbs in the UV region [53]. The reagent was prepared by adding 4.3 mL of $HClO_4$ 70% to a volumetric flask containing 7 mL of water. Then, 33.75 mg of $FeCl_3 \cdot 6H_2O$ were dissolved in the flask and water was added to reach the final volume (25 mL), to obtain a 5 mM concentration of Fe(III). ALN standards in water in the range 5–160 μg/mL were prepared, and the test was carried out by reacting 1 mL of standard/sample with 1 mL of reagent. Spectra were collected with a UV–Vis spectrophotometer Cary3500 (Agilent) in the 280–400 nm range within 30 min from the beginning of the reaction, using integration time 0.02 s, bandwidth 2 nm, and subtracting the contribution of a reference prepared with 1 mL of water and 1 mL of reactant. The absorbance at

300 nm was used to obtain the calibration curve, which is reported in Fig. S2B.

To test whether the presence of gelatin in mixed ALN-gelatin samples might interfere with such spectrophotometric test, we prepared gelatin standards in the concentration range 0.5–10 mg/mL and we tested them with the Fe-based reactant, with the same procedure described for ALN. We observed that in the presence of gelatin concentrations below 2 mg/mL the absorbance at 300 nm is < 0.01, confirming that no interference in the quantification of ALN occurs with this method in the samples we investigated.

Release experiments

Selected specimens prepared with ALN-loaded microparticles (G800_25%_ALN and G500_25%_ALN) were placed on a metallic grid in a glass vial and immersed in 20 mL of MilliQ water, at 37 °C. A small amount of NaN$_3$ was added to water to prevent microbial growth during the experiment. As a reference, sample G0_ALN (see "Preparation of MPCs-gelatin" section) was also tested. At pre-determined times, 1 mL of medium was collected and replaced with 1 mL of MilliQ water, to keep the volume constant. The collected aliquots were stored at 5 °C before analyzing gelatin content (see "Quantification of gelatin" section) and ALN (see "Quantification of ALN" section).

The release curves were fitted according to the Weibull model:

$$\frac{M_t}{M_\infty} = 1 - \exp(-k_w t^{n_w}) \tag{2}$$

where k_w defines the time scale of the process, and n_W is an indicator of the mechanism of release from the matrix ($n_w \leq 0.75$ indicates Fickian diffusion, $0.75 < n_w < 1$ a combination of Fickian diffusion and Case-II transport, $n_w > 1$ indicate a complex release mechanism) [54].

Results and discussion

Characterization of gelatin microparticles

Gelatin microparticles prepared at different stirring speeds were imaged by means of FE-SEM, in order to study both their morphology and size. A representative micrograph and the corresponding size distribution histogram of the single objects observed in each sample are reported in Fig. 1.

Particles obtained at 200 rpm are hundreds of μm-sized and have an irregular and heterogeneous morphology, with a rough surface; as the stirring speed increases, the size decreases up to tens of μm and the particles become more spherical and with a smoother surface. The average diameter of the microparticles, reported in Table 2, was plotted as a function of the stirring speed (see Fig. 2A), revealing a linear relationship between particles' size and stirring speed, up to 800 rpm; out of note, a further increase in the stirring speed (1100 rpm) is not effective in reducing particles' size.

It is worth noting that the size distribution curves in Fig. 1 and the diameters reported in Table 2 are calculated considering the single particles observed in the micrographs; nevertheless, it is evident from SEM images that these particles are partially aggregated. Given that gelatin microparticles were prepared to be used as templating agents for macroporosities in the cement, it is important to characterize the size of the aggregates, as when they are included in the cement formulation the final porosity will be driven by the size of the aggregates. The volume distribution curves determined by laser granulometry are reported in Fig. 2B and Table 2. Consistently with FE-SEM results, the size of the aggregates decreases from sample G200 to G800 (see for instance the D_{50} values in Table 2), while the results for sample G1100 are similar to G800. In all cases, the volume distributions are centered at values of hundreds of μm, suggesting that the prepared microparticles are promising for their use as templating agents to produce, upon dissolution, interconnected macroporosities in the cement whose size range is suitable for cells' penetration and ingrowth.

In order to assess if some olive oil residues were present in the dried gelatin microparticles, the microparticles were studied by means of thermogravimetry. The thermograms, reported in Fig. S3A, were compared with the curve of pristine gelatin: all samples display an additional weight loss below 200 °C, likely due to the loss of water entrapped in the microparticles. Moreover, at 400–420 °C, all samples but G200 show a small peak consistent with the degradation of small amounts of olive oil's residues (see Fig. S3B).
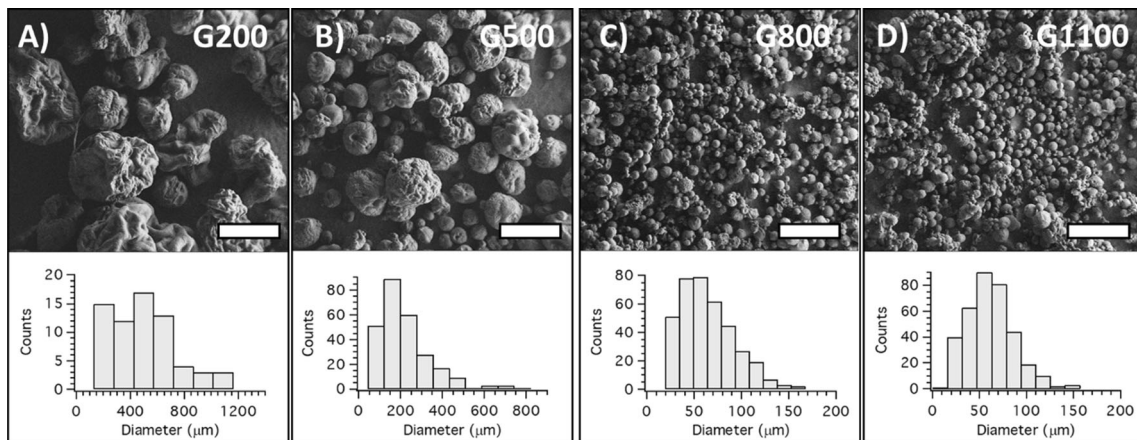
Figure 1 FE-SEM micrographs (top) and size distributions (bottom) of the gelatin microspheres prepared at **A** 200 rpm, **B** 500 rpm, **C** 800 rpm, and **D** 1100 rpm. The scale bar in all SEM images is 500 μm.

Table 2 Size parameters for gelatin microparticles prepared at different stirring speeds

Sample	Diameter (μm)*	SD (μm)*	D_{10} (μm)†	D_{50} (μm)†	D_{90} (μm)†
G200	491	243	420 ± 15	775 ± 45	1450 ± 189
G500	218	127	161 ± 3	318 ± 7	565 ± 28
G800	64	28	81 ± 1	230 ± 8	600 ± 50
G1100	61	25	102 ± 3	300 ± 13	616 ± 33

*Average diameters and standard deviations as obtained from the FE-SEM images

†Values obtained by means of laser granulometry measurements
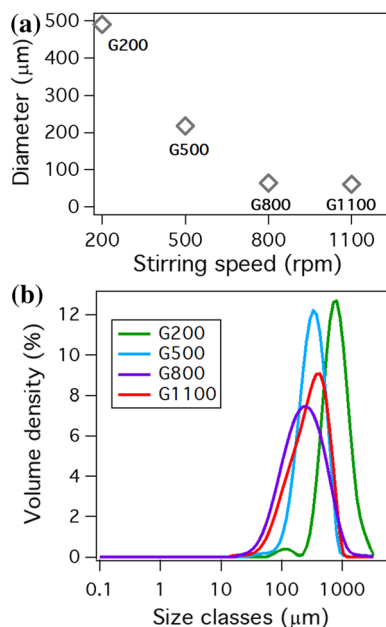
Figure 2 a Plot of gelatin microparticles' diameter estimated from FE-SEM micrographs vs stirring speed used during the synthesis. **b** Volume distribution curves of gelatin microparticles as obtained from laser granulometry measurements.

To sum up, we demonstrated that a simple W/O emulsion method allows for the obtainment of gelatin microspheres whose size can be tuned by varying the stirring speed. The use of olive oil as the continuous phase in the W/O emulsion and the absence of potentially toxic surfactants make suitable the biomedical application of the cement composite. The observed formation of hundreds of μm-sized aggregates is not detrimental for their use as templating agents for porosities in cements, as their dissolution in physiological conditions can lead to the formation of interconnected macroporosities and create an environment favorable for cell permeation and growth. Since G200 are very irregular and heterogeneous and G1100 are comparable to G800, only samples G500 and G800 were selected as porogens to prepare MPCs.

Characterization of cement pastes

G500 and G800 samples have been selected to prepare 5%, 15% and 25% (see Table 1) macroporous magnesium phosphate-based cements. Handling properties and consistency of the composite pastes

that are of paramount importance for bone cements were preliminary studied to determine how the inclusion of gelatin microparticles hinders the cohesion and moldability of the pastes, possibly hampering their effective use to repair bone fractures or defects. The photographs of the pastes immediately after mixing are shown in Fig. 3 (top). In the "G" samples (cements where gelatin microspheres are included as a powder together with TMP, see "Preparation of MPCs-gelatin" section) the inclusion of gelatin microspheres makes the pastes more compact and cohesive, in a concentration-dependent fashion. The same effect is more evident in the "GS" series, in which the particles were swelled for 10 min in DAHP solution before mixing with TMP (see "Preparation of MPCs-gelatin" section). In this case, samples containing GS800 at 15% and 25% appear crumbled and not cohesive, suggesting that not enough water is present in the formulations to obtain a homogeneous paste. In fact, gelatin microparticles absorb a significant amount of water during the swelling process, hampering the hydration of the inorganic powder and the formation of the cement. Moreover, the comparison of formulations prepared with the same amount of gelatin microparticles show that the presence of gelatin mostly affects those formulations prepared with G800 rather than G500, that contain the same amount of gelatin, suggesting that this effect might be due to the different size of the microparticles, being G800 significantly smaller than G500. The higher number of particles present in the G800 samples results in a larger specific surface area interacting with water and limiting its availability for the cement hydration.

Another critical feature of bone cements is their injectability, which makes possible to apply them in micro-invasive surgeries to precisely fill a cavity or a fracture [5]. We qualitatively tested the injectability of pastes by manually injecting them through a syringe 3 min after the mixing, and the results are shown in Fig. 3 (bottom). All formulations but G500_15% and G500_25% of the "G" series are easily injectable, and no phase separation is observed; on the contrary, only one formulation of the "GS" series (GS500_5%) is injectable. Therefore, in these conditions, the inclusion of the dried microparticles with respect to the swollen ones ensures better handling properties and injectability of the paste. For this reason, we decided not to further characterize "GS" samples and to focus our attention on the "G" series.

The setting time of the pastes was evaluated by means of the Gillmore test, and the results reported in Fig. S4 show that the inclusion of gelatin microparticles in the formulations does not significantly affect the setting time of the MPC paste, which is in all cases about 8 min for t_1 (initial setting time) and about 15 min for t_2 (final setting time), therefore within the ideal range defined for calcium phosphate-based bone cements [8].

Characterization of set cements

After setting at 37 °C, all cements are hard and compact and retain the shape of the mold (see Fig. S5). This suggests that up to 25% microparticles do not prevent the formation of an extended cement network, likely due to the good dispersion within the paste during the mixing process.
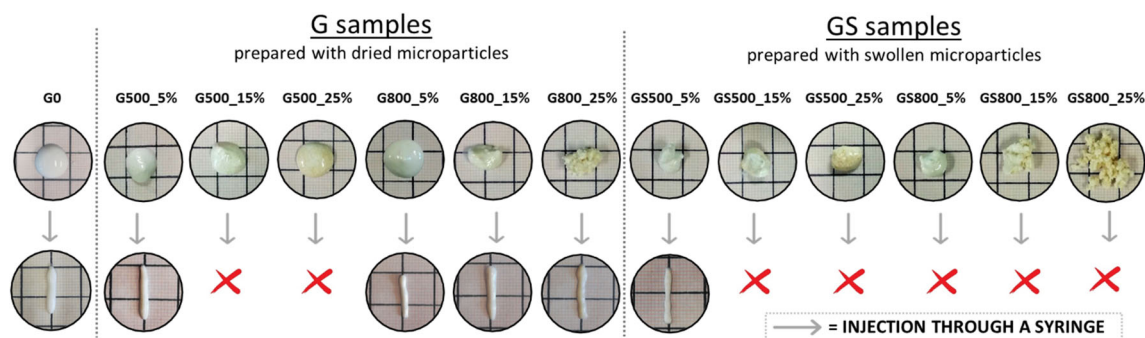

Figure 3 Cement pastes immediately after mixing (top) and after injection through a 2 mL syringe with a 14G conical needle (bottom). Samples from the "G" series (i.e., gelatin microspheres mixed as powder with TMP before the addition of DAHP solution) are on the left, and those from the "GS" series (i.e., gelatin microspheres swelled for 10 min in DAHP solution before mixing with TMP) on the right.

Cements phases were characterized by means of ATR-FTIR. All signals of the spectrum of G0, in Fig. S6A, are ascribable to the main phases typically constituting MPCs prepared upon reaction of TMP and DAHP solutions, i.e., struvite ($MgNH_4PO_4·6H_2O$, which is the reaction product) and unreacted TMP. In particular, the O–H stretching, N–H stretching and bending from struvite [55] and P–O stretching due to both struvite and TMP [55, 56] are present in the ATR-FTIR spectra. The spectra of the cements containing gelatin microparticles, shown in Fig. S7, are not significantly different from G0, and gelatin signals (see Fig. S6B) are not visible, likely due to its small amount and overlap with MPCs' absorption.

Additional information on the morphology of cements were obtained by means of FE-SEM. At low magnifications, sample G0 appears compact and homogeneous (see Fig. S8A), while in high magnification micrographs crystals with struvite's typical morphology are observed (see Fig. S8B) [57]. The morphology of MPCs including gelatin microparticles is shown in Fig. 4. All samples display porosities of tens of μm, and it is possible to observe partially dissolved gelatin microspheres (as in Fig. 4A and C) and interconnected holes due to the presence of

Figure 4 FE-SEM micrographs of MPCs-gelatin samples. The scale bar in all micrographs is 50 μm.

gelatin microparticles dissolved during the setting process at 37 °C (see in particular Fig. 4E and F). The interconnection is evident in specific regions of the sample, where some holes connecting different pores are visible (see Fig. S9). It is expected that a further gelatin dissolution will occur upon incubation of the cements in water, improving the interconnection and the porosity of the material (see "Characterization of set cements" section).

The characterization of samples morphology and chemical composition was also carried out by means of confocal Raman microscopy, and the results for the cross sections of samples G0, G500_25% and G800_25% are shown in Fig. 5. White light images were first collected (see Fig. S10). On the length scale investigated, G0 shows a compact morphology while samples containing gelatin microparticles present several holes likely due to regions where gelatin microspheres were present during the setting process.

Raman maps were obtained by collecting spectra in a selected region (180 × 100 μm) and analyzing specific signals of the Raman spectra, diagnostic of samples' components. The Raman spectra of pure gelatin, struvite and TMP are shown in Fig. 5A. The signal-to-baseline intensity in the highlighted regions was used to obtain the Raman maps, reported in Fig. 5B–D. For G0, the map shows the distribution of the two phases constituting the sample, i.e., TMP and struvite that are the reactant and the main product of MPC reaction. On the micrometric scale, the two phases appear well segregated, as areas rich in struvite lack of TMP and vice versa. MPCs containing gelatin microparticles show additional regions where gelatin signals are present, confirming that the observed holes are due to regions where gelatin microparticles were present and, in this sample, partly dissolved during the setting process at 37 °C.

To sum up, micrometric gelatin particles can be successfully included in magnesium phosphate-based cements. The microparticles enhance the cohesion of the cement pastes and affect their injectability, which is entirely preserved only for G800 particles. Despite the inclusion of gelatin microparticles, the setting time of the cements is within the recommended range for orthopedic applications [8], and the set cements are compact and retain their shape. The phase composition of the cements is preserved in the presence of gelatin microparticles that act as porogen, as confirmed by
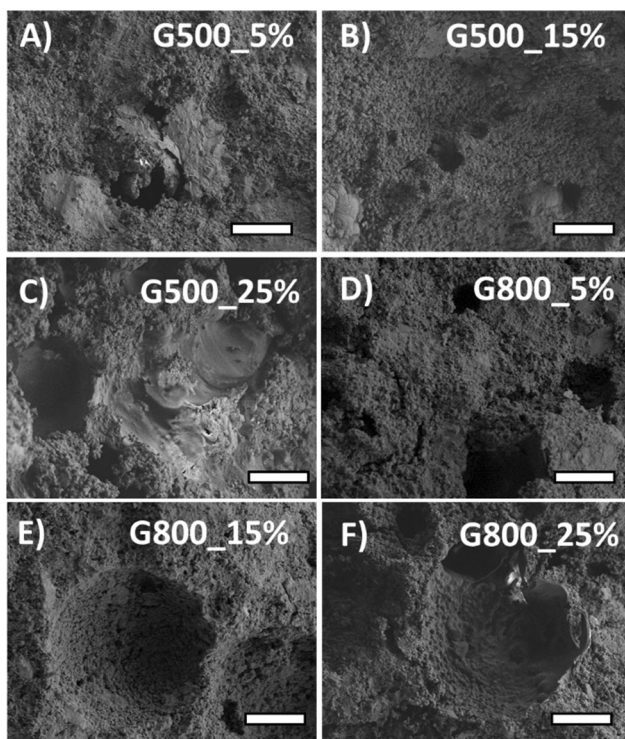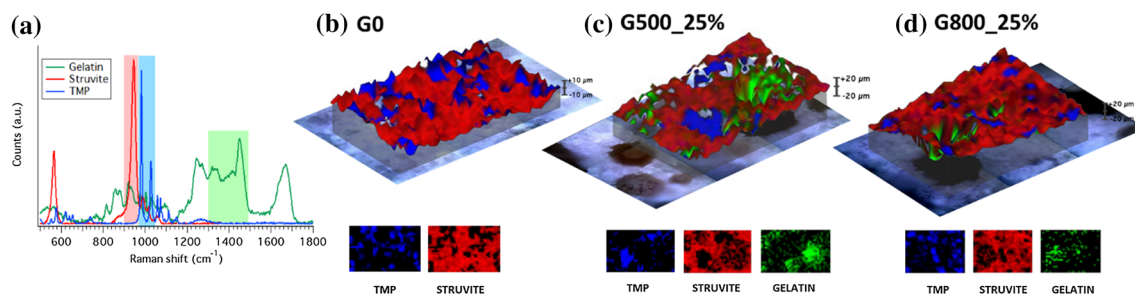
Figure 5 a Raman spectra of the samples' components, where the highlighted regions were used to obtain the 3D maps shown in **b** G0, **c** G500_25% and **d** G800_25%.

FE-SEM and confocal Raman. Moreover, the setting process at 37 °C allows for the partial dissolution of gelatin microspheres which leads to the presence of pores from tens to hundreds of μm in diameter.

Cement incubation in water

In order to understand the fate of the prepared materials when put in a physiological environment, samples were incubated in water at 37 °C. For this series of experiments, MPCs prepared with ALN-loaded microparticles were used. The presence of ALN is not expected to affect MPCs features. The loading % was determined by analyzing the microparticles by means of thermogravimetry and comparing them with the thermograms of pure gelatin and ALN (see Fig. S11). Given that at 1000 °C gelatin loses 100% of its initial weight while ALN loses only about 52%, any residue at 1000 °C in the loaded microparticles can be attributed to the presence of ALN. The comparison of loaded and un-loaded G500 (Fig. S12A) and G800 (Fig. S12B) microparticles reveals a loading % of 20% and 22%, respectively.

G500_ALN and G800_ALN were also characterized by means of laser granulometry, to understand if the loading procedure (see "Preparation of gelatin microparticles and loading with alendronate" section) resulted in an aggregation of gelatin particles. The obtained curves (see Fig. S13) show that some aggregation of the microparticles occurs, but the higher size of G500 (D$_{50}$ 616 μm for G500_ALN) with respect to G800 (D$_{50}$ 366 μm for G800_ALN) is preserved also for the loaded particles.

MPCs prepared with ALN-loaded microparticles were incubated in water to assess both the stability of the cement matrix and the dissolution of gelatin. The observation of samples revealed an excellent stability

and integrity of the cementitious matrix (see Fig. S14), as confirmed also by the weight losses of the material after 12 days calculated according to Eq. 1 and reported in Table 3. The amount of gelatin and ALN present in the incubation medium at the end of the experiment was also examined by means of two distinct spectrophotometric methods (Biuret method for gelatin, see "Quantification of gelatin" section, and Fe(III) method for ALN, see "Quantification of ALN" section). The results reported in Table 3 show that small amounts of gelatin are released from the cement matrix due to the dissolution of the microspheres. In the process, ALN molecules loaded within the microparticles are also released, and its amount is proportional to the amount of microspheres included in the cement. This evidence suggests that the amount of released ALN can be tuned according to the amount of loaded microspheres included in the cement.

The fracture surfaces of the dried specimens after incubation were also examined by means of FE-SEM, to inspect the internal structure and the porosity after incubation (see Fig. 6). Sample G0 is not modified by the incubation in water, as it is evident by observing Fig. S15.

Table 3 Results of the dissolution test

Sample	Weight loss (%)	Gelatin (mg)	ALN (mg)
G0	1.2	–	–
G500_5%_ALN	1.6	0.6	1.9
G500_15%_ALN	2.5	4.2	2.5
G500_25%_ALN	2.3	13.1	3.1
G800_5%_ALN	0.5	0.7	0.6
G800_15%_ALN	2.2	0.7	1.5
G800_25%_ALN	6.8	5.1	3.7

On the other hand, all other samples, particularly those prepared with a high amount of microparticles, show the presence of many pores whose size ranges from tens to hundreds of μm. In some regions, the pores appear very close one to each other, revealing the successful templating action of gelatin microparticles for the obtainment of interconnected macroporosities.

After the dissolution experiments, samples G0 and G800_25%_ALN were also imaged by means of X-ray micro–computed tomography, to inspect the internal structure of the material. Sample G0 (see Fig. 7A) shows a very compact structure, and the few holes observed can be ascribed to air bubbles entrapped in the paste during the setting process. The presence of light and dark areas is due to the different contrast toward X-rays of TMP and struvite, the two phases constituting the samples. From the analysis of the image, we can extrapolate the total porosity of the sample, which is 0.3%, with a closed porosity value of 0.03%. In contrast, sample G800_25%_ALN shows several pores, due to dissolved gelatin microparticles or entrapped air bubbles. In addition, the sample is penetrated throughout its volume by cracks that connect the larger pores present, likely caused by the action of gelatin particles that, upon incubation in water, swell and increase their volume, thus partially
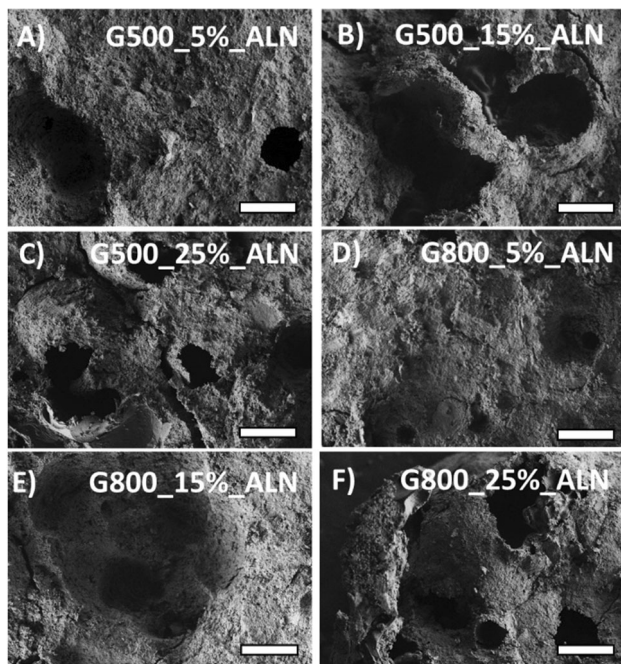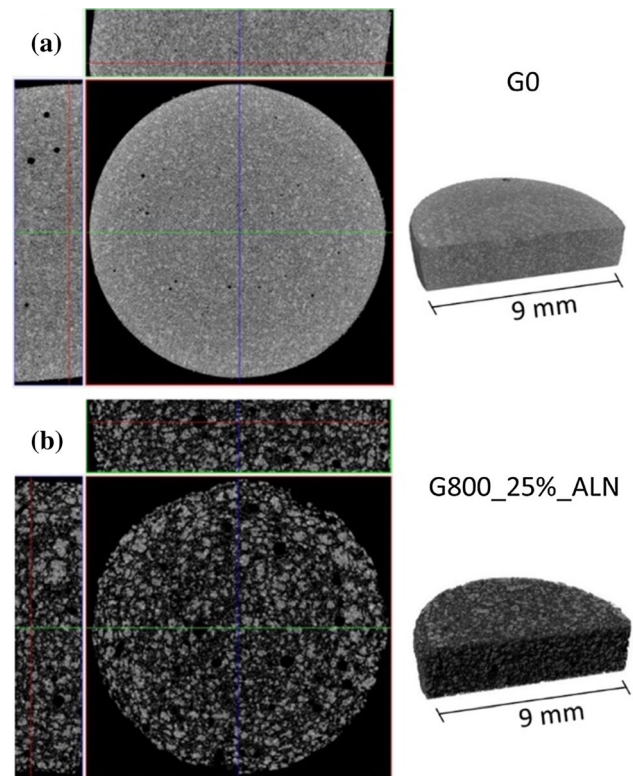

Figure 7 3D computed X-ray microtomography images (3D rendering) and section images of samples G0 (**a**) and G800_25%_ALN (**b**) after dissolution experiment.

disrupting the cement matrix. In this case, the analysis of the image leads to a total porosity of the sample of 42.5%, with only 0.13% of closed porosity. This means that the sample displays a strong degree of interconnection between the pores. Micro-CT thus confirms the porous and interconnected structure of MPCs prepared with gelatin microparticles as templating agents.

Alendronate release experiments

In order to investigate the release kinetic of gelatin and ALN from the cements, samples G0_ALN, G500_25%_ALN and G800_25%_ALN were immersed in water at 37 °C and aliquots of the incubation medium were analyzed as described in the "Materials and Methods" section. We recall that sample G0_ALN was prepared as a reference by mixing ALN powder directly with the cement precursor (see "Preparation of MPCs-gelatin" section). The results of the release experiment are reported in Fig. 8, together with samples' appearance at the end of the experiment (see Fig. 8A). As far as gelatin

Figure 6 FE-SEM micrographs of cements after incubation in water at 37 °C for 12 days. Scale bar: 100 μm.

release is concerned (see Fig. 8B), both G500_25%_ALN and G800_25%_ALN release only about 40% and 30% of its content, respectively, reaching the plateau value in few days. The fitting of the release curves with the Weibull model (see "Quantification of gelatin" section and Fig. S16) suggests a Fickian diffusion mechanism for the process ($n_w < 0.75$, see Table S1).

ALN curves (see Fig. 8C) reveal that the drug can be effectively released from the composite: samples prepared with gelatin microspheres show an analogous release kinetic for ALN, while sample G0 is able to release a slightly higher % of the drug, likely due

to the direct incorporation in the cement matrix rather than in the microparticles. Also in this case, the fittings of the curves with the Weibull model (see Fig. S17 and Table S1), are compatible with a Fickian release process. It is worth mentioning that only about 10% of the ALN included in the composite is released within the time-frame investigated, likely because of the interaction of the molecule with both gelatin and the cement inorganic matrix; nevertheless, it is well known that during an in vivo resorption process, phosphate-based bone cements undergo a complex resorption mechanism [58], sometimes referred to as passive (i.e., solubility-driven) and active (i.e., cell-mediated) [59]. We can hypothesize that in the in vivo application, the resorption process mediated by osteoclasts might contribute to a further ALN release, resulting in a prolonged therapeutic action.

In conclusion, these experiments confirm the two-fold action of gelatin microparticles on MPCs which act both as porogens being released in water upon incubation at 37 °C and as carriers for the loading and local release of ALN.

Figure 8 a Photographs of the samples at the end of the release experiment; **b** release curves for gelatin in samples G500_25%_ALN (green triangles) and G800_25%_ALN (blue squares). **c** ALN release curves in samples G0_ALN (orange dots), G500_25%_ALN (green triangles) and G800_25%_ALN (blue squares).

Conclusions

This work reports a new strategy to produce macroporosity in MPCs which consists in the introduction of gelatin microparticles that, upon dissolution at physiological conditions, are able to generate pores from tens to hundreds of μm, fundamental to ensure bone cells penetration and ingrowth. A simple W/O emulsion method was used to prepare gelatin particles of different size by varying the stirring speed during the synthesis, using olive oil as continuous phase. The microparticles were characterized in terms of composition, size, and shape, finding that smaller and more spherical particles are obtained at high stirring speed. The partial aggregation observed with SEM and granulometry, that for certain applications might be regarded as an issue, in this context should not be considered a drawback as gelatin is used as a templating agent for the creation of interconnected micron-sized porosities. Particles prepared at 500 rpm and 800 rpm were included at different amounts in cements prepared by reacting TMP and DAHP and exploring two different preparation protocols. The effect of the amount and the size of gelatin microparticles on the handling properties,

injectability and setting time of the pastes was assessed, while set cements were characterized by combining ATR-FTIR, SEM and confocal Raman microscopy. In summary, the results show that gelatin microparticles can be effectively included in MPCs, and do not affect the crystallinity of the phases. Their presence in cement matrix results in the presence of macropores likely formed during the setting process at 37 °C. MPCs were then incubated in water at physiological temperature to assess the fate of the materials in conditions compatible with their potential application. For these experiments, gelatin particles were loaded with alendronate, a drug well-recognized for the treatment of osteoporosis. The characterization of the morphology of the cements, recovered after the experiment, shows the interconnection and macroporosity of the cement, as observed by means of SEM and Micro-CT, confirming the dissolution of gelatin. Despite the dissolution of the polymer, cements are able to retain their shape, envisioning a structural integrity of the material when applied in bone. The release profiles of both gelatin and ALN from the cementitious matrix were finally investigated by means of spectrophotometric methods, showing the effectiveness of the designed material for the local release of ALN.

In conclusion, the material described in this work successfully overcomes the main limitations of conventional MPCs, i.e., lack of macroporosity and poor drug release properties [15], by including templating ALN-loaded gelatin microparticles in the cement matrix.

Acknowledgements

Funding

Declarations

Conflict of interest There is no conflict of interest to declare.

Supplementary Information: The online version contains supplementary material available at https://doi.org/10.1007/s10853-022-07439-7.

References

[1] Bigi A, Boanini E (2018) Calcium phosphates as delivery systems for bisphosphonates. J Funct Biomater 9:6. https://doi.org/10.3390/jfb9010006

[2] Qu H, Fu H, Han Z, Sun Y (2019) Biomaterials for bone tissue engineering scaffolds: a review. RSC Adv 9:26252–26262. https://doi.org/10.1039/C9RA05214C

[3] Codrea CI, Croitoru A-M, Baciu CC et al (2021) Advances in osteoporotic bone tissue engineering. J Clin Med 10:253. https://doi.org/10.3390/jcm10020253

[4] Zhang J, Liu W, Schnitzler V et al (2014) Calcium phosphate cements for bone substitution: chemistry, handling and mechanical properties. Acta Biomater 10:1035–1049. https://doi.org/10.1016/j.actbio.2013.11.001

[5] O'Neill R, McCarthy HO, Montufar EB et al (2017) Critical review: Injectability of calcium phosphate pastes and

cements. Acta Biomater 50:1–19. https://doi.org/10.1016/j.actbio.2016.11.019

[6] Yousefi A-M (2019) A review of calcium phosphate cements and acrylic bone cements as injectable materials for bone repair and implant fixation. J Appl Biomater Funct Mater 17:2280800019872594. https://doi.org/10.1177/2280800019872594

[7] Vert M, Doi Y, Hellwich K-H et al (2012) Terminology for biorelated polymers and applications (IUPAC recommendations 2012). Pure Appl Chem 84:377–410. https://doi.org/10.1351/PAC-REC-10-12-04

[8] Dorozhkin SV (2012) Self-setting calcium orthophosphate formulations: cements, concretes, pastes and putties. Int J Mater Chem 1:1–48. https://doi.org/10.5923/j.ijmc.20110101.01

[9] Ostrowski N, Roy A, Kumta PN (2016) Magnesium phosphate cement systems for hard tissue applications: a review. ACS Biomater Sci Eng 2:1067–1083. https://doi.org/10.1021/acsbiomaterials.6b00056

[10] Haque MA, Chen B (2019) Research progresses on magnesium phosphate cement: a review. Constr Build Mater 211:885–898. https://doi.org/10.1016/j.conbuildmat.2019.03.304

[11] Nabiyouni M, Brückner T, Zhou H et al (2018) Magnesium-based bioceramics in orthopedic applications. Acta Biomater 66:23–43. https://doi.org/10.1016/j.actbio.2017.11.033

[12] Wu L, Feyerabend F, Schilling AF et al (2015) Effects of extracellular magnesium extract on the proliferation and differentiation of human osteoblasts and osteoclasts in coculture. Acta Biomater 27:294–304. https://doi.org/10.1016/j.actbio.2015.08.042

[13] Kanter B, Vikman A, Brückner T et al (2018) Bone regeneration capacity of magnesium phosphate cements in a large animal model. Acta Biomater 69:352–361. https://doi.org/10.1016/j.actbio.2018.01.035

[14] Bercier A, Gonçalves S, Lignon O, Fitremann J (2010) Calcium phosphate bone cements including sugar surfactants: part one—porosity, setting times and compressive strength. Materials 3:4695–4709. https://doi.org/10.3390/ma3104695

[15] Kazakova G, Safronova T, Golubchikov D et al (2021) Resorbable Mg2+-containing phosphates for bone tissue repair. Materials 14:4857. https://doi.org/10.3390/ma14174857

[16] Lodoso-Torrecilla I, van den Beucken JJJP, Jansen JA (2021) Calcium phosphate cements: optimization toward biodegradability. Acta Biomater 119:1–12. https://doi.org/10.1016/j.actbio.2020.10.013

[17] Schröter L, Kaiser F, Stein S et al (2020) Biological and mechanical performance and degradation characteristics of calcium phosphate cements in large animals and humans. Acta Biomater 117:1–20. https://doi.org/10.1016/j.actbio.2020.09.031

[18] Vásquez Niño AF, dos Santos LAL, Vásquez Niño AF, dos Santos LAL (2016) Preparation of an injectable macroporous α-TCP cement. Mater Res 19:908–913. https://doi.org/10.1590/1980-5373-MR-2016-0229

[19] Montufar EB, Traykova T, Gil C et al (2010) Foamed surfactant solution as a template for self-setting injectable hydroxyapatite scaffolds for bone regeneration. Acta Biomater 6:876–885. https://doi.org/10.1016/j.actbio.2009.10.018

[20] Miao X, Hu Y, Liu J, Wong AP (2004) Porous calcium phosphate ceramics prepared by coating polyurethane foams with calcium phosphate cements. Mater Lett 58:397–402. https://doi.org/10.1016/S0167-577X(03)00510-X

[21] Xu HHK, Weir MD, Burguera EF, Fraser AM (2006) Injectable and macroporous calcium phosphate cement scaffold. Biomaterials 27:4279–4287. https://doi.org/10.1016/j.biomaterials.2006.03.001

[22] Xu HH, Quinn JB, Takagi S et al (2001) Strong and macroporous calcium phosphate cement: effects of porosity and fiber reinforcement on mechanical properties. J Biomed Mater Res 57:457–466. https://doi.org/10.1002/1097-4636(20011205)57:3%3c457::aid-jbm1189%3e3.0.co;2-x

[23] Barralet JE, Grover L, Gaunt T et al (2002) Preparation of macroporous calcium phosphate cement tissue engineering scaffold. Biomaterials 23:3063–3072. https://doi.org/10.1016/S0142-9612(01)00401-X

[24] Shariff KA, Tsuru K, Ishikawa K (2016) Fabrication of interconnected pore forming α-tricalcium phosphate foam granules cement. J Biomater Appl 30:838–845. https://doi.org/10.1177/0885328215601939

[25] Fu X, Lai Z, Lai X et al (2016) Preparation and characteristics of magnesium phosphate cement based porous materials. Constr Build Mater 127:712–723. https://doi.org/10.1016/j.conbuildmat.2016.10.041

[26] Zhenyu L, Yang H, Xiaojie F et al (2018) Preparation of porous materials by magnesium phosphate cement with high permeability. Adv Mater Sci Eng 2018:1–7. https://doi.org/10.1155/2018/5910560

[27] Jie W, Zhenyu L, Xin H et al (2021) Porous materials prepared by magnesium phosphate cement for the effective immobilization of lead ions. Int J Environ Res 15:681–694. https://doi.org/10.1007/s41742-021-00344-y

[28] Yue L, Bing C (2015) New type of super-lightweight magnesium phosphate cement foamed concrete. J Mater Civ Eng 27:04014112. https://doi.org/10.1061/(ASCE)MT.1943-5533.0001044

[29] Babaie E, Lin B, Bhaduri SB (2017) A new method to produce macroporous Mg-phosphate bone growth

substitutes. Mater Sci Eng C 75:602–609. https://doi.org/10.1016/j.msec.2017.02.111

[30] Ewald A, Lochner B, Gbureck U et al (2012) Structural optimization of macroporous magnesium phosphate scaffolds and their cytocompatibility. Key Eng Mater 493–494:813–819. https://doi.org/10.4028/www.scientific.net/KEM.493-494.813

[31] Alipal J, Mohd-Puad NAS, Lee TC et al (2021) A review of gelatin: properties, sources, process, applications, and commercialisation. Mater Today Proc 42:240–250. https://doi.org/10.1016/j.matpr.2020.12.922

[32] Elzoghby AO (2013) Gelatin-based nanoparticles as drug and gene delivery systems: reviewing three decades of research. J Controlled Release 172:1075–1091. https://doi.org/10.1016/j.jconrel.2013.09.019

[33] Li L, Du Y, Yin Z et al (2020) Preparation and the hemostatic property study of porous gelatin microspheres both in vitro and in vivo. Colloids Surf B Biointerfaces 187:110641. https://doi.org/10.1016/j.colsurfb.2019.110641

[34] Habraken WJEM, de Jonge LT, Wolke JGC et al (2008) Introduction of gelatin microspheres into an injectable calcium phosphate cement. J Biomed Mater Res A 87A:643–655. https://doi.org/10.1002/jbm.a.31703

[35] Nezafati N, Farokhi M, Heydari M et al (2019) In vitro bioactivity and cytocompatablity of an injectable calcium phosphate cement/silanated gelatin microsphere composite bone cement. Compos Part B Eng 175:107146. https://doi.org/10.1016/j.compositesb.2019.107146

[36] Cai S, Zhai Y, Xu G et al (2011) Preparation and properties of calcium phosphate cements incorporated gelatin microspheres and calcium sulfate dihydrate as controlled local drug delivery system. J Mater Sci Mater Med 22:2487–2496. https://doi.org/10.1007/s10856-011-4432-2

[37] Li M, Liu X, Liu X, Ge B (2010) Calcium phosphate cement with BMP-2-loaded gelatin microspheres enhances bone healing in osteoporosis: a pilot study. Clin Orthop Relat Res 468:1978–1985. https://doi.org/10.1007/s11999-010-1321-9

[38] Kiminami K, Nagata K, Konishi T et al (2018) Bioresorbability of chelate-setting calcium-phosphate cement hybridized with gelatin particles using a porcine tibial defect model. J Ceram Soc Jpn 126:71–78. https://doi.org/10.2109/jcersj2.17197

[39] Yamamoto S, Matsushima Y, Kanayama Y et al (2017) Effect of the up-front heat treatment of gelatin particles dispersed in calcium phosphate cements on the in vivo material resorption and concomitant bone formation. J Mater Sci Mater Med 28:48. https://doi.org/10.1007/s10856-017-5861-3

[40] Link DP, van den Dolder J, van den Beucken JJJP et al (2009) Evaluation of an orthotopically implanted calcium phosphate cement containing gelatin microparticles. J Biomed Mater Res A 90:372–379. https://doi.org/10.1002/jbm.a.32091

[41] Habraken WJEM, Boerman OC, Wolke JGC et al (2009) In vitro growth factor release from injectable calcium phosphate cements containing gelatin microspheres. J Biomed Mater Res A 91A:614–622. https://doi.org/10.1002/jbm.a.32263

[42] Zhao Y, Yu S, Wu X et al (2021) Construction of macroporous magnesium phosphate-based bone cement with sustained drug release. Mater Des 200:109466. https://doi.org/10.1016/j.matdes.2021.109466

[43] Fasolino I, Soriente A, Ambrosio L, Raucci MG (2020) Osteogenic and anti-inflammatory behavior of injectable calcium phosphate loaded with therapeutic drugs. Nanomaterials 10:1743. https://doi.org/10.3390/nano10091743

[44] Jindong Z, Hai T, Junchao G et al (2010) Evaluation of a novel osteoporotic drug delivery system in vitro: alendronate-loaded calcium phosphate cement. Orthopedics. https://doi.org/10.3928/01477447-20100625-15

[45] Shen Z, Yu T, Ye J (2014) Microstructure and properties of alendronate-loaded calcium phosphate cement. Mater Sci Eng C 42:303–311. https://doi.org/10.1016/j.msec.2014.05.043

[46] Li Y-H, Wang Z-D, Wang W et al (2015) The biocompatibility of calcium phosphate cements containing alendronate-loaded PLGA microparticles in vitro. Exp Biol Med 240:1465–1471. https://doi.org/10.1177/1535370215579142

[47] Zhao J, Tang H, Wang J, Li G (2014) Local treatment of osteoporosis with alendronate-loaded calcium phosphate cement. Chin Med J (Engl) 127:3906–3914

[48] Panzavolta S, Torricelli P, Bracci B et al (2010) Functionalization of biomimetic calcium phosphate bone cements with alendronate. J Inorg Biochem 104:1099–1106. https://doi.org/10.1016/j.jinorgbio.2010.06.008

[49] Patel ZS, Yamamoto M, Ueda H et al (2008) Biodegradable gelatin microparticles as delivery systems for the controlled release of bone morphogenetic protein-2. Acta Biomater 4:1126–1138. https://doi.org/10.1016/j.actbio.2008.04.002

[50] Gelli R, Mati L, Ridi F, Baglioni P (2019) Tuning the properties of magnesium phosphate-based bone cements: effect of powder to liquid ratio and aqueous solution concentration. Mater Sci Eng C 95:248–255. https://doi.org/10.1016/j.msec.2018.10.083

[51] Moseke C, Saratsis V, Gbureck U (2011) Injectability and mechanical properties of magnesium phosphate cements. J Mater Sci Mater Med 22:2591–2598. https://doi.org/10.1007/s10856-011-4442-0

[52] Gornall AG, Bardawill CJ, David MM (1949) Determination of serum proteins by means of the biuret reaction. J Biol Chem 177:751–766. https://doi.org/10.1016/S0021-9258(18)57021-6

[53] Kuljanin J, Janković I, Nedeljković J et al (2002) Spectrophotometric determination of alendronate in pharmaceutical formulations via complex formation with Fe(III) ions. J Pharm Biomed Anal 28:1215–1220. https://doi.org/10.1016/S0731-7085(02)00021-3

[54] Papadopoulou V, Kosmidis K, Vlachou M, Macheras P (2006) On the use of the Weibull function for the discernment of drug release mechanisms. Int J Pharm 309:44–50. https://doi.org/10.1016/j.ijpharm.2005.10.044

[55] Stefov V, Šoptrajanov B, Kuzmanovski I et al (2005) Infrared and Raman spectra of magnesium ammonium phosphate hexahydrate (struvite) and its isomorphous analogues. III. Spectra of protiated and partially deuterated magnesium ammonium phosphate hexahydrate. J Mol Struct 752:60–67. https://doi.org/10.1016/j.molstruc.2005.05.040

[56] Ogorodova LP, Gritsenko YuD, Vigasina MF et al (2020) Natural Magnesium hydrous orthophosphates bobierrite and kovdorskite: FTIR, Raman, thermal, and thermochemical study. Geochem Int 58:189–199. https://doi.org/10.1134/S0016702920020093

[57] Hövelmann J, Stawski TM, Besselink R et al (2019) A template-free and low temperature method for the synthesis of mesoporous magnesium phosphate with uniform pore structure and high surface area. Nanoscale 11:6939–6951. https://doi.org/10.1039/C8NR09205B

[58] Sheikh Z, Abdallah M-N, Hanafi AA et al (2015) Mechanisms of in vivo degradation and resorption of calcium phosphate based biomaterials. Materials 8:7913–7925. https://doi.org/10.3390/ma8115430

[59] Großardt C, Ewald A, Grover LM et al (2010) Passive and active in vitro resorption of calcium and magnesium phosphate cements by osteoclastic cells. Tissue Eng Part A 16:3687–3695. https://doi.org/10.1089/ten.tea.2010.0281

Publisher's Note Springer Nature remains neutral with regard to jurisdictional claims in published maps and institutional affiliations.